Lithuanian Journal of Physics, Vol. **54**, No. 3, pp. 142–149 (2014)

PECULIARITIES OF SECOND HARMONIC GENERATION BY PARAXIAL BEAMS WITH RADIAL / AZIMUTHAL POLARIZATION IN TYPE II NONLINEAR CRYSTAL

P. Stanislovaitis, A. Matijošius, V. Šetkus, and V. Smilgevičius

Department of Quantum Electronics, Faculty of Physics, Vilnius University, Saulėtekio 9–III, LT-10222 Vilnius, Lithuania
E-mail: paulius.stanislovaitis@ff.stud.vu.lt

Received 17 April 2014; accepted 29 May 2014

In this work we investigate the light patterns generated by paraxial radial and azimuthal polarization beams in type-II nonlinear crystal. We show that in paraxial case the second harmonic intensity pattern generated by the radial / azimuthal polarization beams can be expressed similarly to the Hermite-Gaussian HG_{11} mode. In addition, numerical simulations were carried out taking into account diffraction, walk-off, and pump depletion. The numerical simulations have shown that even with pump depletion the resulting second harmonic beam consists of 4 maxima. Also, experimental results are presented, which confirm theoretical predictions. Interference patterns indicate phase shifts of π between neighbouring maxima.

Keywords: radial / azimuthal polarization beams, Hermite-Gaussian mode, second harmonic generation

PACS: 42.60.Jf, 42.65.Ky, 42.79.-e

1. Introduction

Polarization of light is one of the factors determining the character of lightmatter interaction. Conventionally, laser light can have linear, circular, or elliptical polarization. In these cases the polarization of light is homogeneous, i. e. the polarization of light is the same in a plane perpendicular to the propagation of the beam. Such beams are very easy to obtain by using conventional optical elements (waveplates, polarizers, etc.).

However, it is possible to produce light beams with spatially inhomogeneous polarization. Such beams can induce very different effects when it comes to lightmatter interaction. One class of such spatially inhomogeneous beams are the cylindrical vector (CV) beams, which have cylindrical symmetry. For the first time CV beams were demonstrated in 1972 [1], when a radial polarization beam was produced inside a laser resonator by use of a special mode selector. However, intensive research of CV beams started only in 1999, when unique properties of CV beams were discovered and possible applications started to emerge.

It has been shown that under sharp focusing the beams with radial polarization can be focused into a smaller spot than conventional beams with homogeneous polarization [2–4]. In addition to that, it was also discovered that the sharply focused radially polarized beams have a large longitudinal electric field component [2, 4], which leads to a new kind of light-matter interaction. These properties have been utilized in numerous applications.

Peculiarities of laser material processing using CV beams have been investigated in [5, 6]. In [5] it was shown that the radially polarized beam was the most effective in cutting. The cutting speed and depth were increased by 1.5–2 times compared to beams with the conventional homogeneous polarization.

The use of CV beams in optical tweezers was investigated in [7, 8]. In work [8], the stable 3-dimensional trapping of metallic particles was demonstrated by using CV beams. Metallic particles are difficult to trap using conventional optical tweezers due to strong scattering and absorption forces. Other, more exotic applications include interferometry [9] and electron acceleration [10].

However, little attention has been paid to nonlinear optics of CV beams. There have been some papers dedicated to harmonic generation of CV beams [11, 12]. In work [11], the second and third harmonics produced by CV beams are investigated theoretically. Work [12] deals with nonlinear interaction of CV beams in the sharp focusing regime.

This paper is dedicated to the second harmonic generation (SH) of CV beams in the paraxial regime, in

type-II nonlinear crystals. The SH generation pumped by a CV beam is analysed theoretically and investigated experimentally.

2. Theoretical part

In the paraxial limit, beams with radial and azimuthal polarization are a solution of the paraxial Helmholtz equation in the cylindrical coordinate system [13]. Their intensity distribution is identical to that of Laguerre-Gaussian (LG) 01 mode (1):

$$A_\rho = \frac{A_0}{(1+\mathrm{i}z/l_\mathrm{d})^2}\frac{\rho}{W_0}\exp\left(-\frac{\rho^2}{W_0^2(1+\mathrm{i}z/l_\mathrm{d})}\right), \quad (1a)$$

$$A_\phi = \frac{A_0}{(1+\mathrm{i}z/l_\mathrm{d})^2}\frac{\rho}{W_0}\exp\left(-\frac{\rho^2}{W_0^2(1+\mathrm{i}z/l_\mathrm{d})}\right), \quad (1b)$$

where W_0 is the radius of the Gaussian envelope and $l_\mathrm{d} = \pi W_0^2 n/\lambda$ is the diffractive length, where n is the refractive index. However, in our investigation it is more convenient to write them in the Cartesian coordinate system. In Cartesian coordinates, beams with radial and azimuthal polarization can be expressed as two orthogonally polarized Hermite-Gaussian (HG) 01 and 10 modes:

$$\vec{A}_\rho = \vec{x}_0 A_{\mathrm{HG}01} + \vec{y}_0 A_{\mathrm{HG}10}, \quad (2a)$$

$$\vec{A}_\phi = \vec{x}_0 A_{\mathrm{HG}01} + \vec{y}_0 A_{\mathrm{HG}10}, \quad (2b)$$

where $A_{\mathrm{HG}10}$ and $A_{\mathrm{HG}01}$ are complex amplitudes of the corresponding HG modes:

$$A_{\mathrm{HG}01} = \frac{A_0}{(1+\mathrm{i}z/l_\mathrm{d})^2}\frac{x}{W_0}\exp\left(-\frac{x^2+y^2}{W_0^2(1+\mathrm{i}z/l_\mathrm{d})}\right), \quad (3a)$$

$$A_{\mathrm{HG}10} = \frac{A_0}{(1+\mathrm{i}z/l_\mathrm{d})^2}\frac{y}{W_0}\exp\left(-\frac{x^2+y^2}{W_0^2(1+\mathrm{i}z/l_\mathrm{d})}\right). \quad (3b)$$

Next comes the propagation of a CV beam in a nonlinear crystal. Pump depletion and walk-off are neglected in this analysis. The type-II interaction is assumed. As initial conditions, we have chosen a CV beam with mixed polarization that has both radial and azimuthal polarization components. To express relative magnitude of radial and azimuthal components, we introduce "weight coeficients" α and β that are real and obey the relation $\alpha^2 + \beta^2 = 1$. Using these coefficients, the amplitude of the beam that is superposition of beams with radial and azimuth polarization can be written as follows:

$$A_\mathrm{H} = \frac{\alpha x + \beta y}{W_0(1+\mathrm{i}z/l_\mathrm{H})^2}\exp\left(-\frac{x^2+y^2}{W_0^2(1+\mathrm{i}z/l_\mathrm{H})}\right), \quad (4a)$$

$$A_\mathrm{V} = \frac{\alpha y - \beta x}{W_0(1+\mathrm{i}z/l_\mathrm{V})^2}\exp\left(-\frac{x^2+y^2}{W_0^2(1+\mathrm{i}z/l_\mathrm{V})}\right), \quad (4b)$$

where l_H and l_V are the difractive lengths of the vertical and horizontal polarization components (since the beam propagates in anisotropic medium, they may not be the same).

Keeping in mind the assumptions that were made previously, we start our analysis with the following equation:

$$\frac{\partial A_2}{\partial z} = \frac{\mathrm{i}}{2k_2}\nabla_\mathrm{T}^2 A_2 + \mathrm{i}\sigma_2 A_\mathrm{H} A_\mathrm{V} \mathrm{e}^{-\mathrm{i}\Delta kz}, \quad (5)$$

where A2 is the complex amplitude of the SH beam, σ is the nonlinear interaction coeficient, and ∇_T^2 is the transverse component of the Laplacian:

$\nabla_\mathrm{T}^2 = \frac{\partial^2}{\partial x^2} + \frac{\partial^2}{\partial y^2}$ and k_2 is the wavenumber of the SH beam. To make equations less cumbersome, we introduce the following quantities:

$$X = \frac{x}{W_0}, \quad (6a)$$

$$Y = \frac{y}{W_0}, \quad (6b)$$

$$Z = \frac{2z}{l_{\mathrm{d}2}}, \quad (6c)$$

$$\xi = \alpha X + \beta Y, \quad (6d)$$

$$\eta = \alpha Y + \beta X, \quad (6e)$$

$$\kappa = \sigma_2 l_{\mathrm{d}2} A_0^2, \quad (6f)$$

$$q_\mathrm{H} = \frac{1}{1+\mathrm{i}z/l_\mathrm{H}} = \frac{1}{1+\mathrm{i}z\frac{l_{\mathrm{d}2}}{2l_\mathrm{H}}}, \quad (6g)$$

$$q_\mathrm{V} = \frac{1}{1+\mathrm{i}z/l_\mathrm{V}} = \frac{1}{1+\mathrm{i}z\frac{l_{\mathrm{d}2}}{2l_\mathrm{V}}}, \quad (6h)$$

$$q = q_\mathrm{H} + q_\mathrm{V}, \quad (6i)$$

where $l_{\mathrm{d}2} = k_2 W_0^2/2$ is the diffractive length of the SH beam and $k_2 = 2\pi n_{\mathrm{SH}}/\lambda_{\mathrm{SH}}$ is the wavenumber of the SH beam. By using Eqs. (4–6) and some mathemathical

operations, we obtain a modified propagation equation in the transformed coordinate system $\{\xi, \eta\}$:

$$8\frac{\partial A_2}{\partial Z} = \mathrm{i}\nabla_T^2 A_2 + 4\mathrm{i}\kappa q_H^2 q_V^2 \times \\ \times \xi\eta \exp(-q(\xi^2+\eta^2)) \exp\left(-\mathrm{i}\frac{\Delta k l_{d2} Z}{2}\right), \quad (7)$$

where ∇r_T^2 is the new transverse Laplacian in transformed coordinate system:

$$\nabla_{\mathrm{T}}^2 = \frac{\partial^2}{\partial\xi^2} + \frac{\partial^2}{\partial\eta^2}.$$

We seek the solution of Eq. (7) in the form

$$A_2 = Q(Z)\, f(\xi, \eta) \exp(-q(\xi^2 + \eta^2)). \quad (8)$$

The following derivatives appear in Eq. (7):

$$\frac{\partial^2 A_2}{\partial\xi^2} = \left[\frac{\partial^2 f}{\partial\xi^2} - 2qf - 4q\xi\frac{\partial f}{\partial\xi} + 4q^2\xi^2 f\right] \times \\ \times Q\exp(-q(\xi^2+\eta^2)), \quad (9a)$$

$$\frac{\partial^2 A_2}{\partial\eta^2} = \left[\frac{\partial^2 f}{\partial\eta^2} - 2qf - 4q\eta\frac{\partial f}{\partial\eta} + 4q^2\eta^2 f\right] \times \\ \times Q\exp(-q(\xi^2+\eta^2)), \quad (9b)$$

$$\frac{\partial^2 A_2}{\partial Z} = \left[\frac{dQ}{dZ} - \frac{dq}{dZ}(\xi^2+\eta^2)Q\right] \times \\ \times f\exp(-q(\xi^2+\eta^2)). \quad (9c)$$

Derivatives of q can be found from Eqs. (6g–6i):

$$\frac{\partial q_{\mathrm{H}}}{\partial Z} = -\mathrm{i}a_{\mathrm{H}} q_{\mathrm{H}}^2, \quad (10a)$$

$$\frac{\partial q_{\mathrm{V}}}{\partial Z} = -\mathrm{i}a_{\mathrm{V}} q_{\mathrm{V}}^2. \quad (10b)$$

where

$$a_{\mathrm{H}} = l_{\mathrm{d2}}/(2l_{\mathrm{H}}), \quad (11a)$$

$$a_{\mathrm{V}} = l_{\mathrm{d2}}/(2l_{\mathrm{V}}). \quad (11b)$$

Eqs. (11) reduce to $a_{\mathrm{H}} = n_2/n_{\mathrm{H}}$ and $a_{\mathrm{V}} = n_2/n_{\mathrm{V}}$, where n_2 is the refractive index of the SH beam and n_{V} and n_{H} are refractive indices of the vertical and horizontal polarization components of the first harmonics (FH), respectively. We will assume that the difference between the refractive indices is very small, so that the approximation $a_{\mathrm{H}} \approx a_{\mathrm{V}} \approx 1$ is valid. From this approximation it follows that $q_{\mathrm{V}} \approx q_{\mathrm{H}}$. Using these approximations, we obtain the following relation (12):

$$2\frac{\partial q}{\partial Z} - \mathrm{i}q^2 = -2\mathrm{i}a_{\mathrm{H}} q_{\mathrm{H}}^2 - 2\mathrm{i}a_{\mathrm{V}} q_{\mathrm{V}}^2 + \mathrm{i}q_{\mathrm{H}}^2 + \mathrm{i}q_0^2 + \\ + 2\mathrm{i}q_{\mathrm{H}} q_{\mathrm{V}} \approx 2\mathrm{i}q_{\mathrm{H}} q_{\mathrm{E}} - q_{\mathrm{H}}^2 - q_{\mathrm{V}}^2 = -(q_{\mathrm{H}} - q_{\mathrm{V}})^2. \quad (12)$$

Since $q_{\mathrm{V}} \approx q_{\mathrm{H}}$, the quantity $(q_{\mathrm{H}} - q_{\mathrm{V}})$ is very small. Keeping this in mind and inserting the derivatives (Eqs. (9)), we obtain the following equation:

$$8f\frac{dQ}{dZ} = \mathrm{i}Q\left(\frac{\partial^2 f}{\partial\xi^2} + \frac{\partial^2 f}{\partial\eta^2}\right) - 4\mathrm{i}qQ\left(f + \xi\frac{\partial f}{\partial\xi} + \eta\frac{\partial f}{\partial\eta}\right) + \\ + 4\,\mathrm{i}\kappa q_{\mathrm{H}}^2 q_{\mathrm{V}}^2 \xi\eta \exp\left(-\mathrm{i}\frac{\Delta k l_{\mathrm{d2}} Z}{2}\right). \quad (13)$$

We can see that if we choose $f = \xi\eta$, all members with ξ and η disappear from Eq. (13), since

$$\xi\frac{\partial f}{\partial\xi} + \eta\frac{\partial f}{\partial\eta} = 2\xi\eta, \quad (14a)$$

$$\frac{\partial^2 f}{\partial\xi^2} + \frac{\partial^2 f}{\partial\eta^2} = 0. \quad (14b)$$

Therefore, what remains of Eq. (13) is just the longitudinal part:

$$2\frac{dQ}{dZ} + 3\mathrm{i}qQ = \mathrm{i}\kappa q_{\mathrm{H}}^2 q_{\mathrm{V}}^2 \exp\left(-\mathrm{i}\frac{\Delta k l_{\mathrm{d2}} Z}{2}\right). \quad (15)$$

We introduce quantity $U(Z)$ such that

$$Q(Z) = (q_{\mathrm{V}} q_{\mathrm{H}})^{3/2} U(Z). \quad (16)$$

Remembering the approximation that $a_{\mathrm{H}} \approx a_{\mathrm{V}} \approx 1$ and using Eqs. (10), we obtain the equation for $U(Z)$:

$$\frac{dU}{dZ} = \mathrm{i}\frac{\kappa}{2}(q_{\mathrm{H}} q_{\mathrm{V}})^{1/2} \exp\left(-\mathrm{i}\frac{\Delta k l_{\mathrm{d2}} Z}{2}\right). \quad (17)$$

Eq. (17) can be integrated numerically. It will not be integrated here. However, one should keep in mind that this equation was obtained using an assumption that the FH beam is not depleted. Therefore, it will not be accurate in case of the high conversion eficiency.

To summarize our results, we looked for a solution of Eq. (5) in form of Eq. (8). We found the transverse part $f(\xi, \eta) = \xi\eta$ and derived the equation for quantity $U(Z)$ that describes the growth of SH magnitude in the propagation direction. Putting it all back into the solution, we obtain the following result:

$$A_2 = \frac{U(Z)}{[(1+\mathrm{i}a_{\mathrm{H}}Z)(1+\mathrm{i}a_{\mathrm{V}}Z)]^{3/2}} \times$$
$$\times \xi\eta \exp\left[-\left(\frac{1}{1+\mathrm{i}a_{\mathrm{V}}Z}+\frac{1}{1+\mathrm{i}a_{\mathrm{H}}Z}\right)(\xi^2+\eta^2)\right]. \quad (18)$$

This solution is given in transformed coordinate system $\{\xi, \eta\}$. The physical meaning of the coordinate transformation given in Eqs. (6d, 6e) is rotation. In the beginning of this chapter "weight coeficients" were introduced that are real and obey the relation $\alpha^2 + \beta^2 = 1$. It is known that $\cos^2\phi + \sin^2\phi = 1$ for any angle ϕ. Let us choose that $\alpha = \cos\phi$ and $\beta = \sin\phi$. In this case, the coordinate transformation can be written in matrix form :

$$\begin{bmatrix} \xi \\ \eta \end{bmatrix} = \begin{bmatrix} \cos\phi & \sin\phi \\ -\sin\phi & \cos\phi \end{bmatrix} \begin{bmatrix} X \\ Y \end{bmatrix}. \quad (19)$$

We can see that the matrix in Eq. (19) is a rotation matrix. Therefore, the relative magnitudes of the radial and azimuthal components in the FH beam determine orientation of the SH intensity pattern. It can be seen from Eq. (18) that intensity pattern is equivalent to that of HG11 mode in rotated Cartesian coordinates $\{\xi, \eta\}$.

This result can be explained qualitatively, as shown in Fig. 1. A superposition of radial and azimuth polarizations gives a mixed CV beam, as shown in Fig. 1 (a). In the lower row (Fig. 1 (b–d)) vertical and horizontal polarization components of are shown. In the type-II interaction, SH is produced from two orthogonal polarization components. As we can see from Fig. 1 (b–d), 6 due to the inhomogeneous polarization of the FH beam, one of the orthogonal components is missing in some areas. Therefore, SH will not be generated in those areas. It can be seen that there are 4 such areas. This explains the HG11 mode structure of the SH beam. Also, it can be seen that the radial polarization (Fig. 1 (c)) beam has both orthogonal polarization components in those places where the mixed polarization CV beam (Fig. 1 (b)) has only one, and vice versa. Therefore, the radial polarization beam will generate SH in those areas where the mixed polarization beam will not. The position of the areas where both orthogonal polarization components are present will depend on a relative magnitude ratio of radial and azimuthal components. This explains the dependency of the orientation angle of the SH beam on the initial magnitude ratio of the FH radial and azimuthal components.

Even though the theoretical analysis was carried out in the constant pump approximation, the qualitative treatment of the problem suggests that the spacial structure of the SH intensity pattern should remain similar even in the presence of pump depletion.

SH generation from a radially polarized beam in the type-II KTP crystal was simulated numerically. Results are shown in Fig. 2. The FH wavelength was

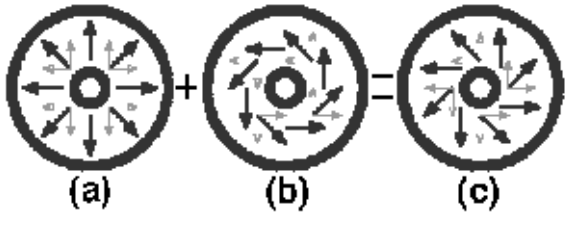

Fig. 1. Qualitative explanation of SH intensity pattern. The polarization of the beam is marked with thick black arrows and the orthogonal components are marked with thin gray arrows: (a) radially polarized beam, (b) azimuthally polarized beam, and (c) superposition product of the beams with radial and azimuthal polarization of equal amplitudes and zero phase difference.

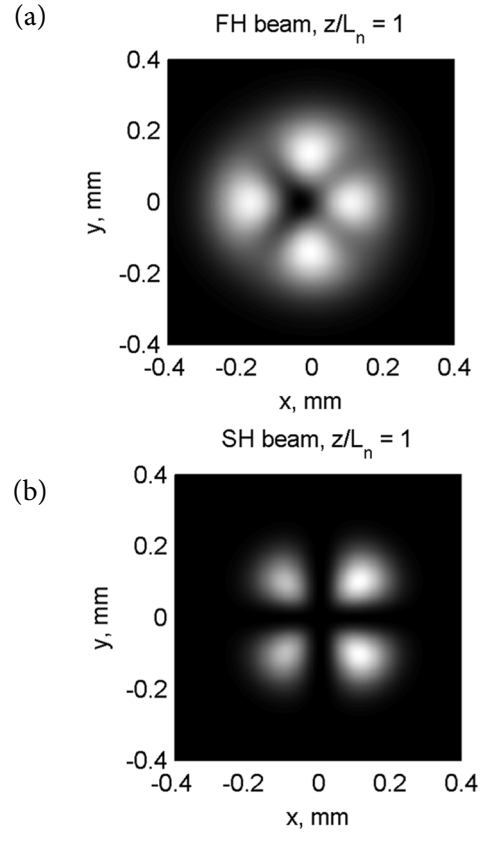

Fig. 2. Numerical results in KTP crystal: (a) FH beam after the SHG interaction (regions of the beam where SH generation took place are depleted) and (b) SH beam (slight assymetry is due to walk-off). L_{n} is the nonlinear length $L_{\mathrm{n}} = \sqrt{\sigma_2 I_0 / 2}^{-1}$ where σ_2 is the nonlinear coupling coeficient of the second harmonic and I_0 is the maximum intensity of the first harmonic beam.

chosen to be 1064 nm. The resulting beam has 4 maxima even in the presence of pump depletion.

3. Experiment

The experimental set-up is shown in Fig. 3. A Nd:YAG nanosecond laser STA-01 (*Standa Ltd*., wavelength 1064 nm) with the TEM_{00} Gaussian profile was used in this experiment. The laser beam, collimated with the lens L1 and polarized with the polarizer P, was split in two branches : the signal beam (*PP*1, *E*, *L*2, *SHC*1, *L*3, *F*1, *M*1) and the reference beam (*M*2, *PP*2, *L*4, *SHC*2, *L*5, *F*2). At the end, the signal and reference beams were recombined and the intensity pattern was recorded with a CCD camera.

The radial polarization element (a.k.a. the S-waveplate) is a $\lambda/2$ waveplate with its principal axis depending on the azimuthal angle. The S-waveplate was manufactured by the direct laser writing in silica glass [14]. By illuminating the volume of glass with ultrashort laser pulses, sub-wavelength nanogratings are formed, which introduce optical anisotropy in material [15, 16]. By distributing these nanogratings with different orientations in the volume of glass, it is possible to create complex polarization elements, which produce beams with inhomogeneous polarization, such as the S-waveplate. The same S-waveplate can generate both radially and azimuthally polarized beams from the linear polarization beam. The resulting beam depends on the polarization direction of the incoming Gaussian beam. For more details on nanograting and S-waveplate operation see references [14–16].

In the signal branch (the bottom branch, as shown in Fig. 3), the CV beam is generated by the use of a specialized polarization converter [14] manufactured by *Altechna R&D*. Then, the *FH* beam is focused with the lens *L*2, a *SH* beam is generated in the *SH* crystal *SHC*1. After filtering off the remains of *FH*, the *SH* beam is imaged on the CCD camera and the intensity pattern is recorded. In the reference branch (the top branch in Fig. 3), a *SH* is generated from an ordinary Gaussian beam. The reference beam was used to produce the interference pattern between the Gaussian and the SH beam generated from the CV beam. The reference beam was used only to measure the intensity pattern and was not used in other parts of the experiment.

The experiment was carried out in three phases:

1) The reference beam was closed and *SH* was generated from the radially polarized beam. An intensity pattern of *HG*11 mode was observed. The recorded intensity pattern is shown in Fig. 4 (a). For comparison, the intensity pattern calculated from Eq. (18) is shown in Fig. 4 (b). Although theoretical analysis was carried out using constant pump approximation, the spatial structure of the *SH* intensity pattern remains the same even with pump depletion. It can be seen from the azimuthal profile (Fig. 4 (d)) that the *FH* beam is depleted in those regions where the *SH* beam has the maximum intensity.

2) The reference beam was opened and the interference pattern between the *SH* beam, generated from CV beam and an ordinary Gaussian beam was recorded with the CCD camera. The interference pattern is shown in Fig. 5. The shift of interference fringes indicates the phase shift of π between the neghbouring maxima.

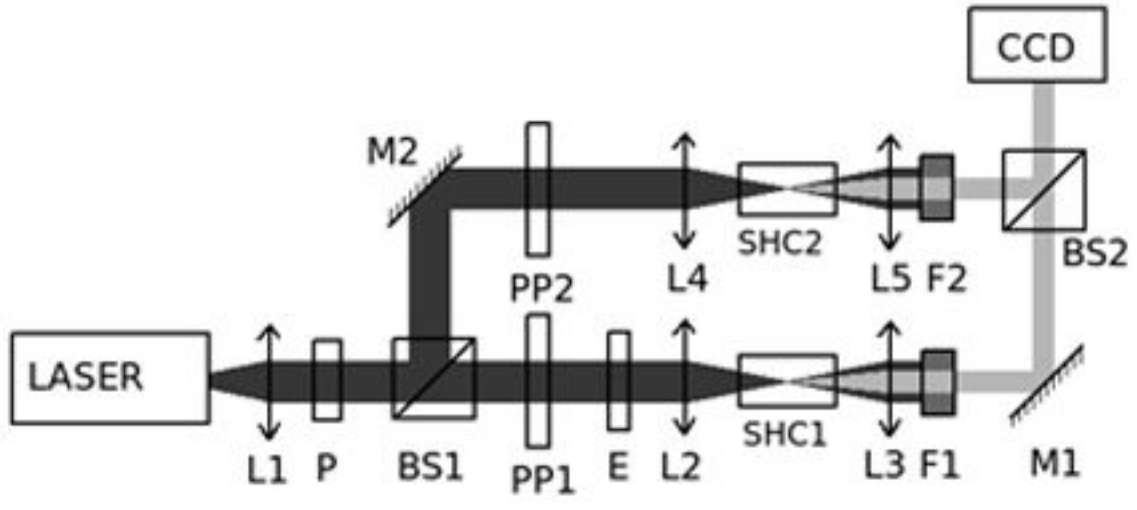

Fig. 3. Experimental set-up: *L*1-*L*5 lens, *BS*1, *BS*2 beam splitters, *M*1, *M*2 mirrors, *P* polarizer, *SHC*1, *SHC*2 SH crystals (KTP), *F*1, *F*2 filters for extracting SH, *E* the radial / azimuthal polarization element, *PP*1 $\lambda/4$ waveplate, *PP*2 $\lambda/2$ waveplate, and *CCD* CCD camera.

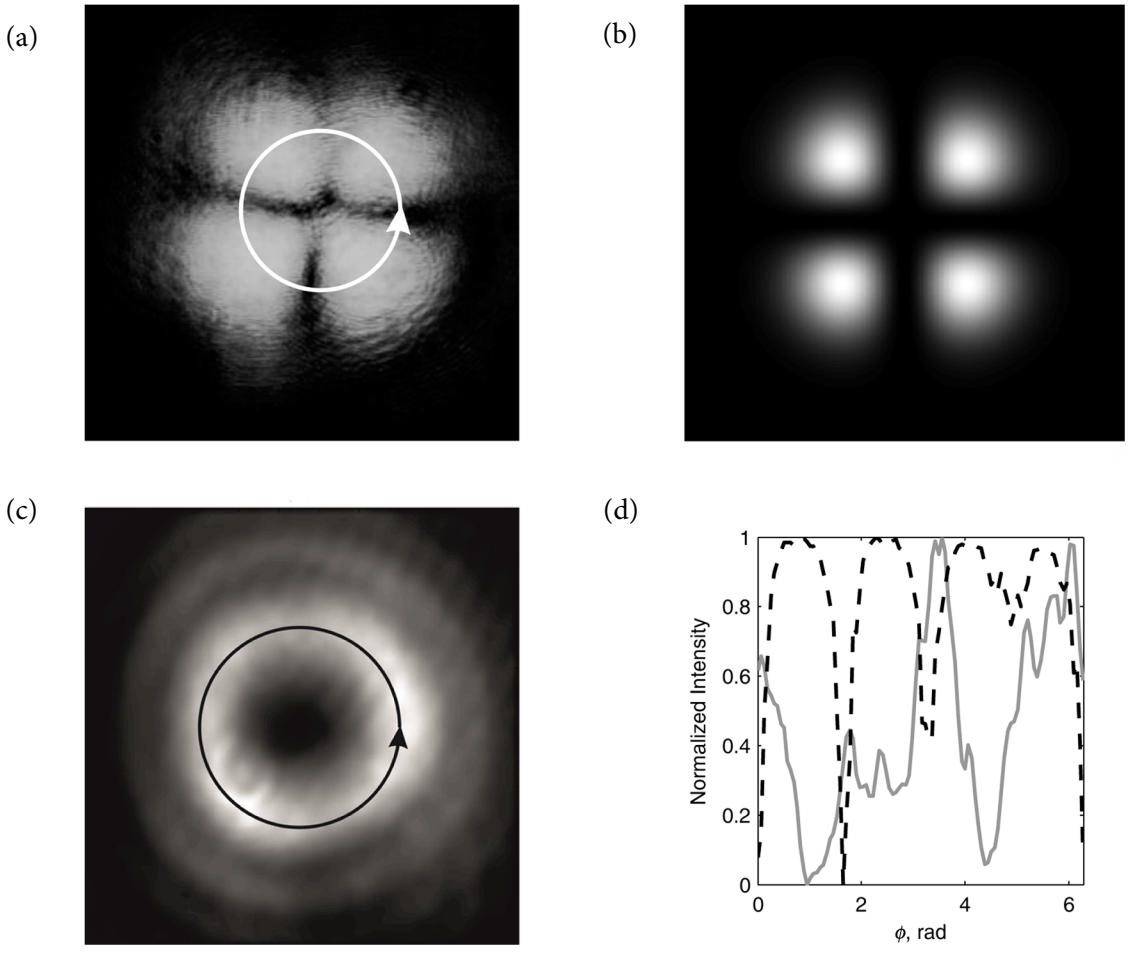

Fig. 4. (a) Experimentally obtained intensity pattern of the SH beam generated from a radially polarized beam. (b) Theoretical result calculated from Eq. (18). (c) FH after interaction beam. (d) Radial profile of the SH (dashed line) and FH (solid line) beams.

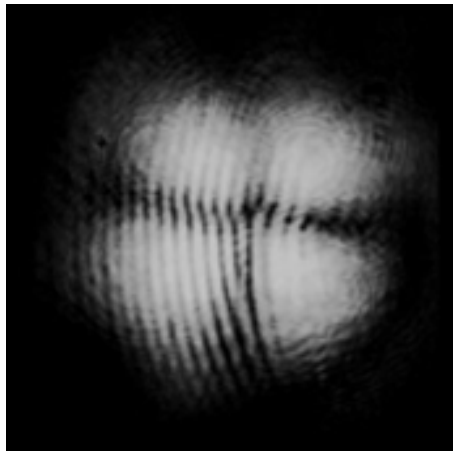

Fig. 5. Interference pattern bewteen a SH generated from the radially polarized beam and an ordinary Gaussian beam. The shift of intensity fringes indicates a phase shift of π between the neighbouring maxima.

3) The reference beam was closed again and by rotating the polarization element *E* a mixed polarization CV beam was produced. The SH intensity pattern from the mixed polarization CV beam was recorded with the CCD camera for several orientations of the polarization element *E*. Rotated intensity patterns were observed with each orientation of the element *E* (Fig. 6).

In addition, efficiency of the second harmonic generation was measured. The eficiency of second harmonic generation from the radially polarized beam was only 25%, while using the same system the eficiency of the second harmonic generation from HG01 mode was 50%. Drop in the eficiency is due to inhomogeneous polarization in the beam. In certain regions, only one polarization component is present, while in the type-II both orthogonal polarization components are required in order to produce the second harmonic.

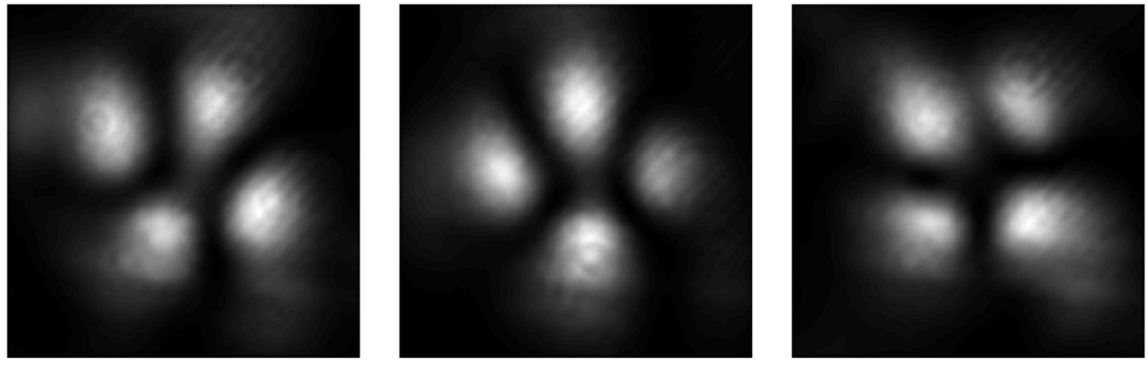

Fig. 6. Second harmonic beams generated form superposition of the beams with radial and azimuthal polarization. This has been achieved by rotating the radial polarization element: (a) 30 deg, (b) 44 deg, and (c) 66 deg.

4. Conclusions

We have investigated the SH generation from a mixed polarization CV beam in the type-II nonlinear crystal. We have shown theoretically that the intensity pattern of the SH beam generated from a CV beam is similar to HG11 mode, consisting of 4 maxima, with the phase differences of π between the neighbouring maxima. This has been verified experimentally by registering an intensity pattern between the SH beam and the Gaussian beam. The shift of interference fringes was observed, indicating the phase shift of π between the neighbouring maxima.

In addition, it was shown theoretically that orientation of the SH beam depends on the relative magnitudes of radially and azimuthally polarized components. This fact has been confirmed experimentally. By rotating the polarization element, the rotation of the SH beam was observed.

Acknowledgement

The study was funded from the European Social Fund under Grant Agreement No. VP1-3.1-MM-08-K-01-004/KS-120000-1756.

References

[1] D. Pohl, Operation of a ruby laser in the purely transverse electric mode TE01, Appl. Phys. Lett. **20**(7), 266–267 (1972), http://dx.doi.org/10.1063/1.1654142

[2] S. Quabis, R. Dorn, M. Eberler, O. Glöckl, and G. Leuchs, Focusing light to a tighter spot, Opt. Commun., **179**(1–6), 1–7 (2000), http://dx.doi.org/10.1016/S0030-4018(99)00729-4

[3] T. Grosjean and D. Courjon, Smallest focal spots, Opt. Commun. **272**(2), 314–319 (2007), http://dx.doi.org/10.1016/j.optcom.2006.11.043

[4] R. Dorn, S. Quabis, and G. Leuchs, Sharper focus for a radially polarized light beam, Phys. Rev. Lett. **91**(23), 233901 (2003), http://dx.doi.org/10.1103/PhysRevLett.91.233901

[5] V.G. Niziev and A.V. Nesterov, Influence of beam polarization on laser cutting efficiency, J. Phys. D Appl. Phys. **32**(13), 1455 (1999).

[6] M Meier, V. Romano, and T. Feurer, Material processing with pulsed radially and azimuthally polarized laser radiation, Appl. Phys. Mater. Sci. Process. **86**(3), 329–334 (2007), http://dx.doi.org/10.1007/s00339-006-3784-9

[7] H. Kawauchi, K. Yonezawa, Y. Kozawa, and S. Sato, Calculation of optical trapping forces on a dielectric sphere in the ray optics regime produced by a radially polarized laser beam, Opt. Lett. **32**(13), 1839–1841 (2007), http://dx.doi.org/10.1364/OL.32.001839

[8] Q. Zhan, Trapping metallic Rayleigh particles with radial polarization, Opt. Express **12**(15), 3377–3382 (2004), http://dx.doi.org/10.1364/OPEX.12.003377

[9] G.M. Lerman and U. Levy, Radial polarization interferometer, Opt. Express **17**(25), 23234–23246 (2009), http://dx.doi.org/10.1364/OE.17.023234

[10] M.O. Scully and M.S. Zubairy, Simple laser accelerator: Optics and particle dynamics, Phys. Rev. A **44**(4), 2656–2663 (1991), http://dx.doi.org/10.1103/PhysRevA.44.2656

[11] S. Carrasco, B.E.A. Saleh, M.C. Teich, and J.T. Fourkas, Second- and third-harmonic generation with vector gaussian beams, J. Opt. Soc. Am. B **23**(10), 2134–2141 (2006), http://dx.doi.org/10.1364/JOSAB.23.002134

[12] A. Ohtsu, Second-harmonic wave induced by vortex beams with radial and azimuthal polarizations,

Opt. Commun. **283**(20), 3831–3837 (2010), doi:http://dx.doi.org/10.1016/j.optcom.2010.04.018

[13] Q. Zhan, Cylindrical vector beams: from mathematical concepts to applications, Adv. Opt. Photon. **1**(1), 1–57 (2009), http://dx.doi.org/10.1364/AOP.1.000001

[14] M. Beresna, M. Gecevičius, P.G. Kazansky, and T. Gertus, Radially polarized optical vortex converter created by femtosecond laser nanostructuring of glass, Appl. Phys. Lett. **98**(20), 201101 (2011), http://dx.doi.org/10.1063/1.3590716

[15] Y. Shimotsuma, P.G. Kazansky, J. Qiu, and K. Hirao, Self-organized nanogratings in glass irradiated by ultrashort light pulses, Phys. Rev. Lett. **91**(24), 247405 (2003), http://dx.doi.org/10.1103/PhysRevLett.91.247405

[16] M. Beresna, M. Gecevičius, and P.G. Kazansky, Polarization sensitive elements fabricated by femtosecond laser nanostructuring of glass, Opt. Mater. Express **1**(4), 783–795 (2011), http://dx.doi.org/10.1364/OME.1.000783

ANTROSIOS HARMONIKOS GENERAVIMO PARAKSIALINIAIS RADIALINĖS / AZIMUTINĖS POLIARIZACIJOS PLUOŠTAIS ANTROJO TIPO NETIESINIAME KRISTALE YPATUMAI

P. Stanislovaitis, A. Matijošius, V. Šetkus, V. Smilgevičius

Vilniaus universiteto Fizikos fakultetas, Kvantinės elektronikos katedra, Vilnius, Lietuva

Santrauka

Darbe ištirti antrosios harmonikos generavimo ypatumai antrojo tipo netiesiniame kristale žadinant ją radialinės / azimutinės poliarizacijos kaupinimo pluoštais. Teoriškai parodyta, kad paraksialiniu atveju generuojamos antrosios harmonikos intensyvumo skirstinys, nepaisant kaupinimo pluoštų nuskurdinimo bei apertūrinio-diafragminio reiškinio, yra išreiškiamas Ermito-Gauso HG11 moda. Atlikus skaitinius modeliavimus, parodyta, kad antrosios harmonikos intensyvumo skirstinys, net ir įskaitant difrakciją, kaupinimo pluoštų nuskurdinimą ir apertūrinį-diafragminį reiškinį, susideda iš keturių maksimumų. Eksperimentinių tyrimų rezultatai patvirtina teorinių skaičiavimų rezultatus. Remiantis užregistruotų interferencinių skirstinių analize nustatyta, kad fazių skirtumas tarp gretimų antrosios harmonikos intensyvumo skirstinio maksimumų yra lygus π radianų.